Quantifying molecular specificity of $\alpha_v\beta_3$ integrin-targeted optical contrast agents with dynamic optical imaging

Michael Gurfinkel
Texas A&M University
Photon Migration Laboratories
College Station, Texas 77843-3012

Shi Ke
Wei Wang
Chun Li
University of Texas M.D. Anderson Cancer Center
Department of Diagnostic Radiology
Houston, Texas 77030

Eva M. Sevick-Muraca
Texas A&M University
Photon Migration Laboratories
College Station, Texas 77843-3012

Abstract. Dynamic fluorescence images were obtained from a subcutaneous human Kaposi's sarcoma tumor (KS1767) model immediately following the intravenous injection of an integrin-targeting cyanine dye conjugate, Cy5.5-c(KRGDf). The fluorescence images, acquired via an intensified charge-coupled device detection system, were used in conjunction with a pharmacokinetic (PK) model to determine kinetic properties of target binding in the presence and absence of a competitive ligand, free c(KRGDf). The results indicate that the conjugate dye behaves similarly in normal tissue to the free Cy5.5 dye while it possesses increased uptake in tumor tissue. The change in pharmacokinetic parameters obtained from dynamic imaging of Cy5.5-c(KRGDf) after administration of c(KRGDf) as a competitive ligand to the integrin receptor suggests that (i) the increased uptake of Cy5.5-c(KRGDf) is molecularly specific and that (ii) receptor turnover occurs within 24 h. In addition, PK analysis enables quantification of an *in vivo* c(KRGDf) binding constant attributable to integrin binding. *In vivo* pharmacokinetic analysis based on rapid and dynamic optical imaging may be potentially useful for evaluating the presence and turnover rate of disease markers that are potential targets of molecular medicine.
[DOI: 10.1117/1.1924696]

Keywords: molecular imaging; pharmacokinetics; cancer; integrin; fluorescence; xenograft.

Paper 04170R received Aug. 30, 2004; revised manuscript received Dec. 5, 2004; accepted for publication Dec. 20, 2004; published online Jun. 7, 2005.

1 Introduction

In the past several years, there has been acceleration in the development of cancer agents which act to inhibit signal transduction that would otherwise lead to the proliferation or antiapoptosis of the cancer cells. The agents are often targeted to an extracellular membrane bound receptor or to an intracellular protein critical to the signaling pathway, resulting in the interruption of the downstream signaling cascade.[1–4] A surrogate marker and noninvasive imaging technique that could assess receptor or protein expression levels could enable (i) evaluation of patient candidacy for receiving the therapeutic agent, (ii) early indication of treatment response, and (iii) understanding of the mechanism of therapeutic responses. The integrin $\alpha_v\beta_3$ has been associated with tumor progression and metastasis[5] and has been shown to play a critical role in tumor angiogenesis.[6] Furthermore, antagonists of $\alpha_v\beta_3$ have been shown to decrease angiogenesis and induce tumor regression in preclinical tumor models.[7,8] Both peptide and antibody integrin antagonists have been clinically evaluated.[9,10] Studies involving peptide or antibody targeting of paramagnetic agents for magnetic resonance imaging[11] or radiotracers for nuclear imaging[12–14] have been reported for predicting treatment outcome or patient candidacy for integrin-targeted therapies. In this work, we demonstrate the use of fast, dynamic optical imaging from which early time pharmacokinetic analyses may provide *in vivo* information of receptor-ligand affinity and receptor expression levels, as well as an estimate of the timescales associated with receptor turnover. The diagnostic agent used was a conjugate of cyclo(Lys-Arg-Gly-Asp-D-phe) peptide [c(KRGDf)], known to selectively bind to $\alpha_v\beta_3$ integrin,[13] and a fluorescing cyanine dye, Cy5.5, for optical imaging of $\alpha_v\beta_3$ integrin overexpressed on xenografted tumors in a murine model of human Kaposi's sarcoma, KS1767, as well as on cultured cells *in vitro*. Upon pretreatment with the c(KRGDf) peptide to occupy the $\alpha_v\beta_3$ integrin receptor sites for binding of the conjugate Cy5.5-c(KRGDf), we show that dynamic optical imaging may be used to provide pharmacokinetic parameters that indicate *in vivo* receptor expression levels as well as their modification in response to therapy.

In the following, we present the materials and methods, derivation of the pharmacokinetic model, as well as the phar-

Address all correspondence to E. M. Sevick-Muraca, Photon Migration Laboratories, Department of Chemistry, P.O. Box 30012, Texas A&M University, College Station, TX 77842; Tel: +1 979 458 3206; Fax: +1 979 458 1011; E-mail: eva-m-sevick@tamu.edu

1083-3668/2005/$22.00 © 2005 SPIE

macokinetic (PK) parameters for uptake of free Cy5.5 and Cy5.5-c(KRGDf) in the absence of and following administration of c(KRGDf) as a blocking ligand within KS1767 and normal tissues *in vivo*. The study is conducted with small subcutaneous tumors on xenografts where tomographic imaging with diffusion-based, time-dependent measurements of light propagation and generation are inappropriate and invalid. Nonetheless, the rapid, continuous-wave measurements permitted by a red-sensitive intensifier coupled with a charge coupled device (CCD) camera provide dynamic imaging from which pertinent PK parameters of molecular specificity can be obtained.

2 Materials and Methods

2.1 *Synthesis Cy5.5-c(KRGDf)]-Conjugate*

c(KRGDf) was synthesized on linker-PL-DMA resin using Fmoc solid phase chemistry as described previously.[15] Briefly, peptide was cleaved from the support with 1% trifluoroacetic acid (TFA) with all sidechain protecting groups intact. The head-to-tail cyclization was then carried out in DMF using benzotriazol-1-yl-oxy-tris-pyrrolidino-phosphonium hexaflurophosphate, 1-hydroxybenzotriazole, and N,N-diisopropylethylamine (DIPEA) as coupling agents. After removal of all sidechain protecting groups the cyclic peptide was purified by reverse phase HPLC eluted with H_2O/acetonitrile containing 0.1% TFA. For conjugation with the fluorescence dye, a solution of Cy5.5-NHS [Eq. (1)] and c(KRGDf)] [Eq. (1.3)] in DMF/DIPEA (10/1,v/v) was stirred at room temperature overnight. After all solvents and by-products were removed under vacuum, the compound was purified by reverse phase HPLC eluted with a 0.01 M solution of NH_4OAc in water/methanol. The Cy5.5-c(KRGDf) product was validated by analytic HPLC and MALDI mass spectrometry.

2.2 *Cell Adhesion Assay*

KS1767 cells were seeded in DMEM/F12 culture medium supplemented with 10% fetal bovine serum for 24 h. Cells (1×10^5) with different concentrations of c(KRGDf) or Cy5.5-c(KRGDf) were added to vitronectin-coated microtiter wells under serum-free conditions and incubated at 37 °C for 1 h. After washing steps, the bound cells were stained with 5% crystal violet, followed by addition of 0.1 M HCl to each well. The concentrations of crystal violet were determined by ultraviolet/visible absorption at 627 nm. IC_{50} values were estimated from the dose-activity curves.

2.3 *Animal Model*

Six-week-old female athymic nude mice (nu/nu; 18–22 g) were purchased from Harlan Sprague Dawley, Inc. (Indianapolis, IN) and housed five per cage and fed sterilized pelleted food (Harlan Sprague Dawley Inc., Indianapolis, IN) and sterilized water. Animals were maintained in a specific pathogen-free mouse colony in the Department of Veterinary Medicine (The University of Texas M. D. Anderson Cancer Center, Houston, TX). The facility is accredited by the American Association for Laboratory Animal Care and all experiments were performed in accordance with the guidelines of the Institutional Animal Care and Use Committee.

Tumor cells to be implanted into mice were harvested near confluence by incubation with 0.05% trypsin-EDTA. Cells were pelleted by centrifugation at $450\times g$ for 5 min and resuspended in sterile PBS. Cells ($2-3\times10^6$/animal) were implanted subcutaneous into the thigh region of mice.

Animals were subdivided into four test groups based on the contrast agent administered. Animals in the first group ($N=2$) received the free Cy5.5 dye (6 nmol/mouse), while animals in the remaining three groups were administered the Cy5.5-c(KRGDf) conjugate (6 nmol/mouse). Of those animals receiving the conjugate dye, one-third received the conjugate dye alone ($N=3$); one-third received the conjugate one hour after the intravenous injection of unconjugated c(KRGDf) peptide ($N=3$); and the remaining third received the conjugate 24 h after the intravenous injection of the unconjugated c(KRGDf) peptide ($N=3$). The unconjugated c(KRGDf) peptide was administered at 200 times the dose of the Cy5.5-c(KRGDf) conjugate.

2.4 *Experimental Imaging Method*

Before fluorescence imaging, mice were anesthetized by intraperitoneal injection of 50 mg $(kg\,bw)^{-1}$ Nembutal (Sigma, St. Louis, MO) and a catheter was positioned into the tail vein to facilitate the subsequent delivery of the fluorescent dye. Fluorescence images were obtained every 7 s for a period of approximately 18 min following the injection of contrast agent. Excitation light provided by a laser diode (660 nm, 35 mW) whose beam was expanded via a planoconvex lens and a holographic diffuser to provide a uniform excitation field of approximately 12 cm in diameter over the surface of the animal. An intensified CCD, comprised of a 16-bit CCD camera (Photometrics, model CH350/L, Tucson, AZ) coupled to an image intensifier (model FS9910C, ITT Night Vision, Roanoke, VA) via a 105 mm lens, functioned as an area detector of re-emitted fluorescence light.[16] A holographic notch-plus band rejection filter (660 nm center wavelength; Kaiser Optical Systems, Inc., Ann Arbor, MI) and a bandpass filter (710 nm center wavelength; CVI Laser, Albuquerque, NM) were positioned prior to a 50 mm lens to reject backscattered and reflected excitation light and isolate only re-emitted fluorescence light. For the acquisition of white-light images, a low-power lamp provided a white-light source and the filters were removed. Image acquisition was controlled by a personal computer equipped with $V++$ imaging software (Digital Optics, Auckland, New Zealand). The first five images were acquired prior to the bolus administration of the fluorescent probe, and thus, served as base line or background images.

The injected dose of Cy5.5-c(KRGDf) and the image exposure time were equivalent to 6 nmol (in 0.3 mL volume) and 800 ms, respectively, and were constant for all the imaging studies conducted. Fluorescence images were obtained at 24 h postinitial injection and again every 24 h thereafter until little or no fluorescence signal was detectable from the tumor region of interest, as determined qualitatively, for up to 168 h.

2.5 *Analysis of Pharmacokinetics from Dynamic Imaging*

Upon completion of the imaging routine, a background image was subtracted from each of the acquired fluorescence images. The white light image was then used to define two re-

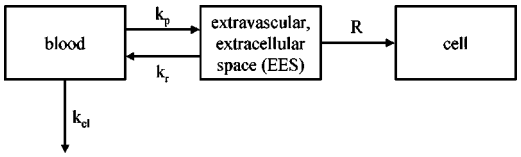

Fig. 1 Schematic depicting the three-compartment pharmacokinetic model employed.

gions of interest (ROI); one was located entirely within the circumference of the tumor and the other, approximately equivalent in size, defined a region of normal tissue located symmetrically opposite the tumor site. Utilizing Matlab software (The MathWorks, Inc., Natick, MA) the mean of the fluorescence intensity within each ROI was computed for every fluorescence image acquired. Plots of mean fluorescence intensity versus time were then generated for each of the imaging studies performed. The mean fluorescence intensity as a function of time after agent administration within each ROI was fitted via a nonlinear Levenberg–Marquardt regression algorithm to the PK equation described in the following section.

3 Theory

3.1 *Derivation of Three-Compartment Pharmacokinetic Model*

In this section we develop a pharmacokinetic model in order to describe the time-dependent distribution of the fluorescing dye-peptide conjugate throughout the animal. The model, depicted schematically in Fig. 1, is comprised of three compartments in which Cy5.5 resides: (i) the blood plasma compartment, (ii) the extravascular, extracellular compartment, and (iii) the tissue compartment representing the ''bound'' Cy5.5 associated to the integrin receptor.

The dye is administered rapidly into the blood plasma compartment via an intravenous bolus injection. From this central blood compartment, the dye diffuses across the vascular endothelium, and partitions into the extravascular, extracellular space (EES) represented by the second compartment. The endothelial transfer coefficient or the rate constant for the distribution of dye from the blood to the EES is given by k_p while k_r is the rate constant describing the reflux from the EES to the blood. A measure of vascular permeability can be obtained from an analysis conducted on first pass circulation data, or data obtained immediately following the bolus injection of the agent. In the past, Cuccia et al. employed a pharmacokinetic analysis to quantify physiologic parameters related to capillary permeability following the administration of the nonspecific dye indocyanine green.[17]

In addition to extravasation into the EES, the dye is eliminated from the blood compartment via other routes such as kidney filtration and liver metabolism, described collectively by the rate constant k_{el}. For nonspecific dyes, that is, dyes that do not exhibit cellular specificity, the blood and EES compartments may be sufficient to describe their distribution.[17,18] However, for dyes that exhibit molecular specificity, a third compartment is included. This third compartment represents the association of the dye at a molecular level, whether it is through surface receptor binding or cellular uptake. The rate at which the dye accumulates in the cellular compartment, whether through association with cellular membrane receptors or internalization, is denoted by R.

If the rate of accumulation of dye in the cellular compartment, R, is constant, determining the time-dependent dye concentration in each of the compartments is relatively straightforward. However, in general, the association between the dye and the cell is a saturable process. Therefore, the rate of dye uptake by the cell may be expressed as

$$R=\frac{V_m C_{\mathrm{EES}}}{K_m+C_{\mathrm{EES}}}, \tag{1}$$

where V_m is the maximum rate of dye internalization or receptor association at the cellular compartment and K_m is known as the Michaelis constant and is equivalent to the dye concentration at which the rate of uptake is equivalent to one-half the maximum rate. Equation (1) is a form of the Michaelis–Menten expression for a saturable reaction based on a single substrate mechanism. Using Eq. (1) to express the rate of distribution of the dye to the cellular compartment leads to nonlinear pharmacokinetics and considerably complicates the mathematics of the model. Fortunately, at low dye concentrations, where C_{EES} is much smaller than K_m, Eq. (1) reduces to

$$R=\frac{V_m}{K_m}C_{\mathrm{EES}}=k_c C_{\mathrm{EES}}, \tag{2}$$

where V_m/K_m can be expressed as an apparent first-order rate constant, k_c, that describes the distribution of dye between the EES and bound, cellular compartments. Furthermore, the distribution of dye from the EES to the cellular compartment is assumed to be a one-way process which is proportional to the available integrin receptor density. That is, cellular uptake is considered irreversible and dissociation of the receptor-dye complex is assumed to occur at a rate much slower than the rate of association. Therefore, the rate constant for the reflux from the cell to the EES compartment is assumed to be negligible. Applying this approximation, the diminution and accumulation of dye in each of the three compartments can be expressed as

$$\frac{dC_B}{dt}=-(k_p+k_{\mathrm{el}})C_B+k_r C_{\mathrm{EES}}=-k_B C_B+k_r C_{\mathrm{EES}}, \tag{3}$$

$$\frac{dC_{\mathrm{EES}}}{dt}=k_p C_B-(k_r+k_c)C_{\mathrm{EES}}=k_p C_B-k_{\mathrm{EES}}C_{\mathrm{EES}}, \tag{4}$$

$$\frac{dC_c}{dt}=k_c C_{\mathrm{EES}}, \tag{5}$$

where $k_B=k_p+k_{\mathrm{el}}$, $k_{\mathrm{EES}}=k_r+k_c$, t is time, and C_B, C_{EES}, and C_C represent the concentration of dye in the blood, EES, and the cell, respectively.

The detected fluorescence intensity at the tissue surface is mediated by a number of factors including the tissue optical properties of scattering and absorption and the depth and concentration of the embedded fluorophore within the tissue. For purposes of monitoring the temporal fluorescence intensity we

can assume optical properties of the tissue are constant and can express the detected fluorescence intensity as a weighted sum of the concentration of the dye in each compartment

$$I(t) \cong w_1 C_B + w_2 C_{\mathrm{EES}} + w_3 C_C, \quad (6)$$

where $I(t)$ is the time-dependent fluorescence intensity and w_1, w_2, and w_3 are weighting functions that represent the volume fraction of the blood, EES, and the cellular compartments, respectively. Additionally, the weighting functions account for the attenuation that occurs as the fluorescent light traverses each compartment.

To obtain the time-dependent dye concentration in each of the compartments, the system of differential equations given by Eqs. (3)–(5) may be solved simultaneously subject to the initial condition that at the time of i.v. bolus injection of the dye, $t=0$, $C_B = C_{\mathrm{Bo}}$, $C_{\mathrm{EES}} = 0$, and $C_c = 0$. The results may then be applied to Eq. (6) to obtain the following expression for the time-dependent observed fluorescence intensity:

$$I(t) = I_0 + A[1 - \exp(-\alpha t)] + B[1 - \exp(-\beta t)], \quad (7)$$

where

$$I_0 = w_1 C_{\mathrm{Bo}}, \quad (8)$$

$$A = \frac{C_{\mathrm{Bo}}}{\alpha - \beta}\left[k_p w_2 - (\alpha - k_{\mathrm{EES}}) w_1 - \frac{k_c k_p w_3}{\alpha}\right], \quad (9)$$

$$B = \frac{C_{\mathrm{Bo}}}{\alpha - \beta}\left[(\beta - k_{\mathrm{EES}}) w_1 - k_p w_2 + \frac{k_c k_p w_3}{\beta}\right], \quad (10)$$

and α and β are complex rate constants given by

$$\alpha = \tfrac{1}{2}[k_{\mathrm{EES}} + k_B + \sqrt{(k_{\mathrm{EES}} - k_B)^2 + 4 k_r k_p}], \quad (11)$$

$$\beta = \tfrac{1}{2}[k_{\mathrm{EES}} + k_B - \sqrt{(k_{\mathrm{EES}} - k_B)^2 + 4 k_r k_p}]. \quad (12)$$

The pre-exponential factors A and B are concentration terms that mathematically reflect the magnitude of the detected signal. Upon inspection of Eqs. (9) and (10) one observes that it is difficult to relate these parameters to physiological parameters as the volume fractions of vascular and extravascular space or the rate constants governing dye uptake. Nonetheless, these parameters may reflect high vascular volumes associated with diseases.

An examination of Eqs. (11) and (12) reveals that the complex rate constant α must be greater than β. As a result, at early time points the expression for the observed fluorescence intensity is more strongly influenced by the term containing α. However, the exponential term containing α approaches zero more rapidly than does the term containing β. Consequently, at later time points the expression for the observed fluorescence intensity becomes a function of β alone. Therefore, the early time portion of the fluorescence intensity profile is referred to as the α phase whereas the later portion is known as the β phase.

Furthermore, it is evident that the values of α and β are intimately related to the values of all other rate constants. It is particularly interesting to examine how α and β vary with the magnitude of the elimination rate constant, k_{el}. For example, if the value of k_{el} is varied while all other rate constants remained fixed, the root function that appears in the expression for both α and β would asymptotically approach $k_B - k_{\mathrm{EES}}$ for large values of k_{el} and $k_{\mathrm{EES}} - k_B$ for small values. As a result, α approaches k_B while β approaches k_{EES} when the intrinsic elimination is very rapid. The trend is reversed when elimination is slow; α approaches k_{EES} while β approaches k_B. Finally, and more importantly, because α and β differ by only the sign in front of the root function, the sum of α and β yields the sum of all rate constants between the various compartments of the model, $\alpha + \beta = k_{\mathrm{el}} + k_p + k_r + k_c$. One may exploit this result to determine the magnitude of the rate constant for specific uptake of contrast agent within the cellular compartment, k_c as follows: for a given specific contrast agent administered in an animal bearing a tumor model in which the specific cellular uptake mechanism has been compromised while the remaining mechanisms of dye uptake remain unchanged, the net decrease in $\alpha + \beta$ reflects the magnitude of the rate constant for specific cellular uptake of the contrast agent.

As a final note, from Eq. (7) it is evident that I_0 represents the fluorescence intensity at the time of contrast agent administration or background fluorescence intensity level. Thus, when one applies a background subtraction technique, the mathematical equivalent of setting I_0 equal to zero, the number of parameters to be fit is reduced such that the time-dependent observed fluorescence intensity may be expressed as

$$I(t) = A[1 - \exp(-\alpha t)] + B[1 - \exp(-\beta t)], \quad (13)$$

where the pharmacokinetic parameters A, B, α, and β were previously defined in Eqs. (9)–(12). Given time-dependent observations of fluorescence intensity, Eq. (13) may be employed in a regression algorithm to obtain estimates of the pharmacokinetic parameters A, B, α, and β.

In summary, the four parameter, double-exponential equation represents the analytical solution to a three-compartment pharmacokinetic model with first order distribution between (i) the vascular, (ii) the extravascular extracellular space, and that associated with (iii) molecularly specific binding. The parameters α and β are complex rate constants governing uptake into each of the three compartments and its sum, $(\alpha + \beta)$ represents the sum of first order rate constants.

4 Results and Discussion

4.1 *In vitro Binding Studies*

To test the antiadhesive activity of Cy5.5-c(KRGDf) and c(KRGDf) peptides, attachment of KS1767 cells (1×10^5) to vitronectin-coated microtiter wells were studied using different concentrations of each peptide. Both Cy5.5-c(KRGDf) and c(KRGDf) behaved similarly, blocking the attachment of KS1767 cells to microtiter wells in a dose-dependent manner with estimated IC_{50} of 2.5 and 1.2 μM, respectively. Figure 2 shows the dose-dependent inhibition of KS1767 cell adhesion as indicated by the diminution of crystal blue dye with increasing concentrations of both Cy5.5-c(KRGDf) and c(KRGDf). Cell attachment was inhibited because the peptides compete for ligand binding sites of the cell surface integrins. These *in vitro* results confirm the molecular specificity of Cy5.5-c(KRGDf) and c(KRGDf) to the cell surface integrins.

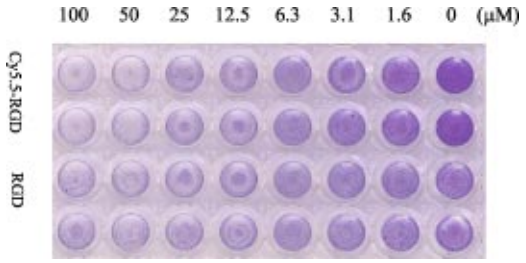

Fig. 2 Dose-dependent inhibition of adhesion of KS1767 cells to vitronectin-coated microplate wells by c(KRGDf) and Cy5.5-c(KRGDf).

Furthermore, using fluorescence microscopy we have confirmed the inhibition of Cy5.5-c(KRGDf) binding to KS1767 cells by preincubation with c(KRGDf).[15]

4.2 *Pharmacokinetic Analysis*

Figure 3 represents typical dynamic fluorescence intensity profiles in the (a) tumor ROI and (b) normal ROI and the corresponding least-squares fit obtained from one representative animal of each of the groups that received an injection of the Cy5.5-c(KRGDf) conjugate. The coefficient of determination R^2 for the regression was 0.99 or greater in all cases. In both normal and tumor ROIs, uptake was (i) greatest when the animal received Cy5.5-c(KRGDf) conjugate alone, (ii) reduced when the animal received the Cy5.5-c(KRGDf) conjugate 1 h after administration of free c(KRGDf) as a blocking agent, and (iii) recovered when the animal received the Cy5.5-c(KRGDf) conjugate 24 h after administration of free c(KRGDf) as a blocking agent. In addition, normal tissue experiences a diminished reduction of update with administration of competitive binding of c(KRGDf) than seen in the Kaposi's sarcoma. This is presumably due to the lower integrin receptor density found in normal tissues as compared to Kaposi's sarcoma.

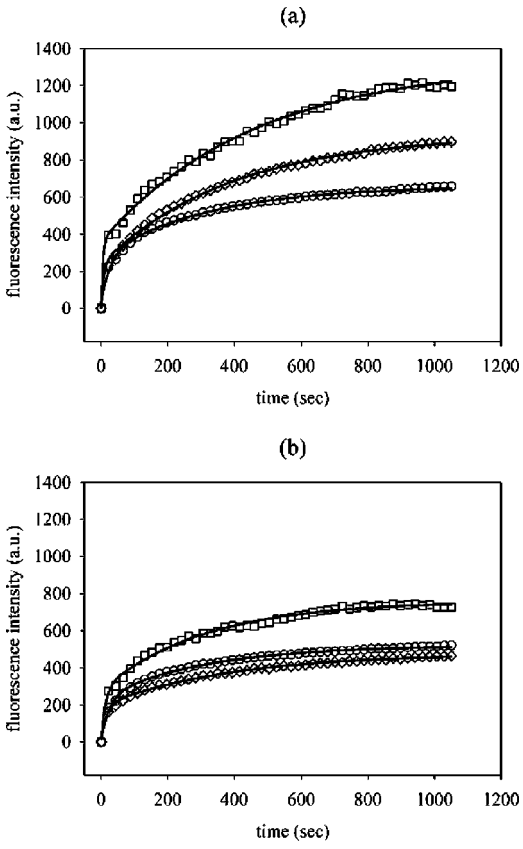

Fig. 3 Fluorescence intensity versus time profiles obtained from one representative animal of each of the groups that received an injection of the RDG-Cy5.5 conjugate, acquired from the (a) tumor ROI and (b) normal ROI. The symbols denote experimental measurements while the solid line denotes the corresponding least-squares fit. The squares (□) denote data from an animal receiving the Cy5.5-c(KRGDf) conjugate alone, while the circles (○) and diamonds (◇) represent data obtained from an animal receiving the conjugate 1 h and 24 h, respectively, after the injection of RGD peptide.

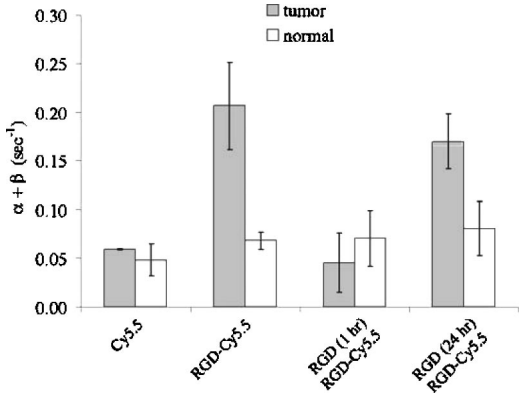

Fig. 4 Results of the nonlinear least-squares regression in determining the sum of the pharmacokinetic complex rate constants $\alpha+\beta$. The column height represents the mean value of the test group listed along the abscissa while the error bars represent the standard deviation. The time in parenthesis represents the time between injection of the RGD peptide and the Cy5.5-c(KRGDf) conjugate.

Figure 4 shows that the sum of the pharmacokinetic rate constants, $\alpha+\beta$, does not appear to differ between the normal ROIs of all animal groups; a series of homoscedastic pooled t tests confirmed that the mean estimates of $\alpha+\beta$ are not significantly different, at a 95% significance level. For animals injected with free Cy5.5 and animals pretreated with c(KRGDf) peptide one hour prior to the injection of the Cy5.5-c(KRGDf) conjugate, the values of $\alpha+\beta$ in tumor ROIs are statistically similar at a 95% level of significance to each other and to the mean values of $\alpha+\beta$ determined from the normal ROIs. These results suggest that the free Cy5.5 dye exhibits similar targeting, or lack thereof, in KS1767 tumor tissue and in normal tissue. In contrast, the value of $\alpha+\beta$ was found to be three to fourfold greater for the tumor ROIs of the animals which received Cy5.5-c(KRGDf) conjugate (mean $\alpha+\beta=0.21$) than for those values (i) from the normal tissue ROIs in animals injected with Cy5.5 or Cy5.5-c(KRGDf) (mean $\alpha+\beta=0.049$ or 0.068) and (ii) from the tumor ROIs in animals injected with Cy5.5 (mean $\alpha+\beta=0.055$). Statistical analysis revealed that the estimates for $\alpha+\beta$ from within the tumor ROIs of the test groups administered Cy5.5-c(KRGDf) alone or the conjugate dye 24 h after treatment with free c(KRGDf) peptide were significantly different from the values of the remaining test groups.

The conjugate Cy5.5-c(KRGDf) exhibited a lack of tumor targeting when the administration of the dye is preceded by the injection of free c(KRGDf) peptide by 1 h, as evidenced by the fact that no statistical difference in $\alpha+\beta$ value was found between the tumor ROIs of animals receiving Cy5.5 dye and that of mice receiving c(KRGDf) followed by Cy5.5-c(KRGDf) 1 h later. When the c(KRGDf) peptide preceded injection of the conjugate by 24 h, the value of $\alpha+\beta$ in tumor ROIs was recovered and became once again significantly different from the $\alpha+\beta$ values of the normal tissue ROIs and from the tumor ROIs of mice injected with Cy5.5 and mice injected with c(KRGDf) followed by Cy5.5-c(KRGDf) with a 1 h interval.

From the studies involving the administration of the RGD peptide prior to the administration of the Cy5.5-c(KRGDf) conjugate, one may draw the following conclusions. First, because the net effect of administering the RGD peptide one hour prior to the Cy5.5-c(KRGDf) conjugate is the reduction of the tumor uptake and since the $\alpha_v\beta_3$ integrin receptor overexpressed on KS1767 binds the RGD peptide, the pharmacokinetic analyses from dynamic imaging verify the specific binding of the Cy5.5-c(KRGDf) conjugate. Second, because the value of $\alpha+\beta$ obtained from the tumor ROIs of animals injected with the conjugate dye alone or the conjugate dye 24 h following the pretreatment with the RGD peptide are statistically similar, one may speculate that the turnover of the $\alpha_v\beta_3$ integrin receptor expressed on the cell surface of KS1767 occurs within 24 h. Given experimental dynamic *in vivo* fluorescence data obtained subsequent to the injection of the Cy5.5-c(KRGDf) conjugate at various intervals following the administration of the c(KRGDf) peptide, one may be able to experimentally determine receptor turnover time. Finally, since $\alpha+\beta$ is equivalent to the sum of all the rate constants of the compartmental pharmacokinetic model, and since the $\alpha_v\beta_3$ integrin receptors bind the c(KRGDf) peptide such that pretreatment with the c(KRGDf) peptide results in the elimination of the cellular uptake of the dye conjugate, the difference in the value of $\alpha+\beta$ between animals injected with the conjugate dye alone and animals injected with the conjugate 1 h after the pretreatment with the RGD peptide may indicate the molecularly specific cellular uptake of the conjugate. Using this rationale, we found the rate constant for the specific cellular uptake of Cy5.5-c(KRGDf) to have a mean value of $k_c = 0.16\ \mathrm{s}^{-1}$.

While the sum of α and β can be used to provide model-dependent information about molecular binding as described earlier, the regression values for the PK complex rate constants, α and β as well as the PK pre-exponential factors A and B are individually presented in Fig. 5. As shown in Figs. 5(a) and 5(b), the complex rate constant, α, is greater than β in these early time-course studies and shows significant differences between normal and tumor tissues when Cy5.5-c(KRGDf) is administered. The differences disappear when Cy5.5-c(KRGDf) is administered 1 h after c(KRGDf) is administered as a blocking ligand, but reappear again when administered 24 h after c(KRGDf) is administered. The complex rate constant, β, does not show significant differences between these groups in the early time courses investigated herein. Further study at longer times after administration of Cy5.5-c(KRGDf) need to be conducted in order to effectively address possible differences. The pre-exponential factors illustrated in the histograms of Figs. 5(c) and 5(d) are truly arbitrary factors which could vary with external factors such as variation in illumination power on the animal surface. Nonetheless, with the exception of the free Cy5.5 dye, the tumor regions possess greater values of the pre-exponential factors indicative of perhaps of the increased vascularity. Clearly, owing to the large number of parameters that constitute α, β, A, and B individually, it is not possible to extract biophysical information in the same manner as one can for the sum of $\alpha+\beta$.

Fluorescence images of all animals studied were also obtained at 24 h intervals following the administration of the contrast agent. Figure 6 displays the images of raw fluorescence (i.e., no background subtraction) overlaid with white light images and obtained 24 and 48 h following the initial injection of the contrast agent for a representative animal of each of the four test groups studied. From the images of Fig. 6(a) it is clear that the KS1767 tumor was not visible from the fluorescence images at any time following the injection of the free Cy5.5 dye. In this case and the other cases as well, the visible fluorescence intensity originating from the animal gut is due to animals' diet. The KS1767 tumor was clearly visible 24 and 48 h after the administration of the Cy5.5-c(KRGDf) peptide, as evidenced in Figs. 6(b)–6(d), and returned to base line after about 168 h. At any given time, the fluorescence intensity originating from the tumor was highest for the animal that was administered the Cy5.5-c(KRGDf) conjugate alone, Fig. 6(b); slightly diminished for the animal injected with the RGD peptide 24 h prior to the administration of the conjugate dye, Fig. 6(d); and lower still for the animal that received the RGD peptide 1 h prior to the administration of the Cy5.5-c(KRGDf) conjugate, Fig. 6(c). These results further substantiate the specific *in vivo* cellular binding of the Cy5.5-c(KRGDf) conjugate to KS1767.

5 Summary and Conclusions

In the past several years, a number of targeted cancer drugs have shown tremendous promise and a select few have been approved by the Food and Drug Administration (FDA). These cancer drugs generally target and inhibit signal transduction that would otherwise lead to the proliferation or antiapoptosis of the cancer cells. The drug is often targeted to an extracellular membrane bound receptor or to an intracellular protein critical to the signaling pathway, resulting in the interruption of the downstream signaling cascade.[1] Herceptin®, developed by Genentech, Inc. and approved by the FDA in 1998, exerts its therapeutic effects on metastatic breast cancer cells that overexpress the HER-2 receptor.[1–3] Similarly, Erbitux®, developed by ImClone Systems Inc., targets the extracellular membrane-bound epidermal growth factor receptor, commonly overexpressed in many types of cancer.[1,2] More recently, the protein-tyrosine kinase Bcr-Abl, whose elevated activity is strongly implicated in the mechanism of development of chronic myeloid leukemia, has been the molecular target of a therapeutic drug.[4] The drug, Gleevec®, marketed by Novartis Pharmaceutical Corporation in 2001, competitively binds the ATP binding site on the enzyme, and suppresses the proliferation of Bcr-Abl-expressing cells.[1–4]

An ongoing challenge for drug discovery is the unmet need for (i) rapid *in vivo* animal screening tools in order to verify

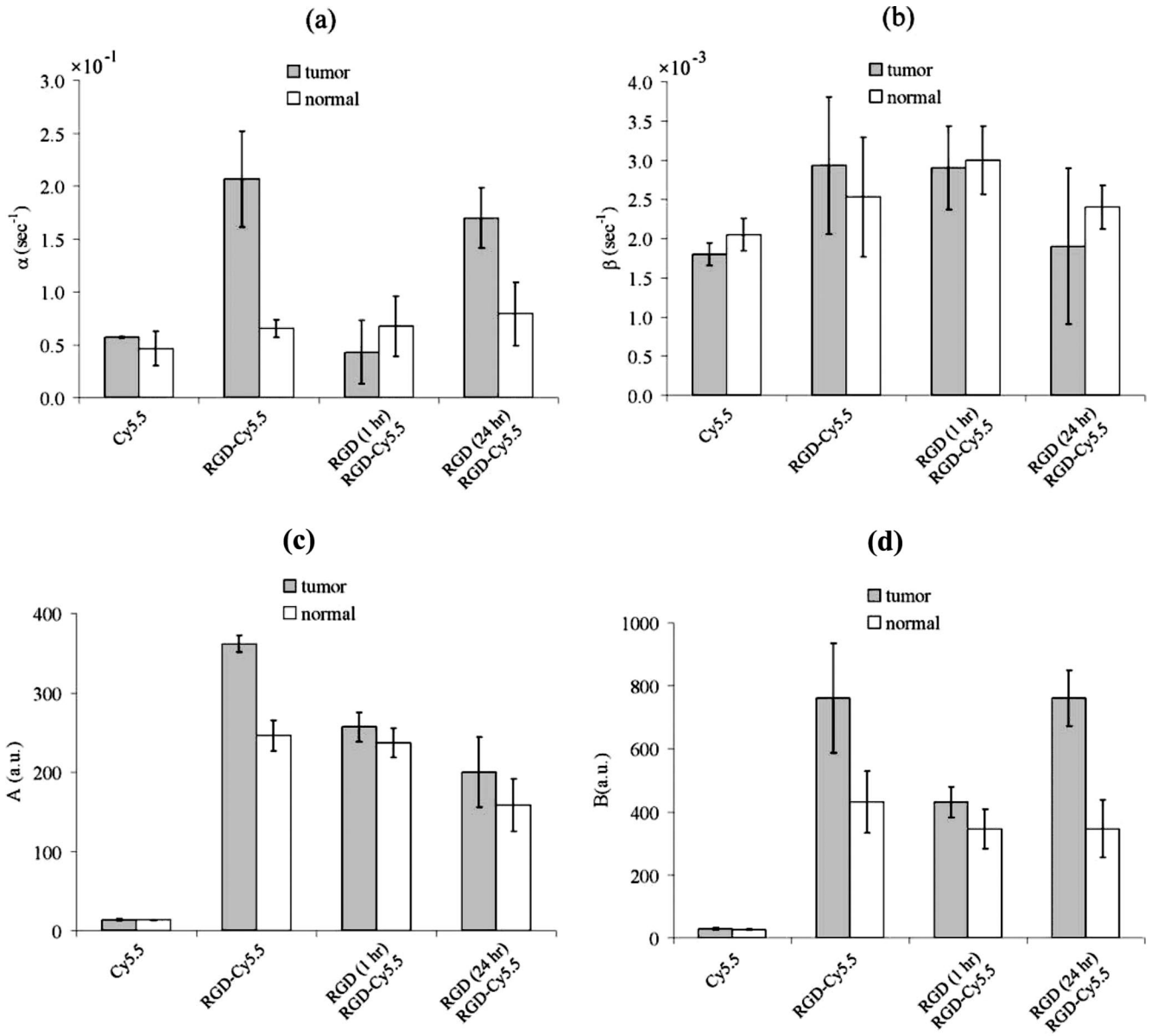

Fig. 5 Results of nonlinear least-squares regression for determining the PK complex rate constants (a) α and (b) β as well as the PK pre-exponential factors (a) A and (b) B from Eq. (13). The column height represents the mean value of the test group listed along the abscissa while the error bars represent the standard deviation. The time in parentheses represents the time between injection for the c(KRGDf) peptide and the Cy5.5-c(KRGDf) conjugate. Figure 5(b) is similar to Fig. 4 owing to the small values of β.

molecular targeting and action and (ii) candidate patient screening in phase II and III clinical trials in order to decrease their durations and to improve their efficiency. While diffusion-based fluorescence enhanced tomography has been demonstrated for clinically relevant volumes,[19–23] to date RTE-based tomographic algorithms valid for small animal imaging remains to be developed. Herein, we have shown that before such developments, a sensitive and simple optical technique capable of rapid collection of dynamic measurements can provide information of molecular update without the need for tomography or quantification of tissue fluorophore concentration. Upon combining dynamic measurements and pharmacokinetic analysis with proper controls and competitive *in vivo* ligand binding studies, the molecular specificity of any small targeted agent can be determined *in vivo* relative to a nonspecific analog such as in the case of a conjugate containing a scrambled, nonspecific peptide. In addition, by assessing the change in the uptake kinetics of a molecularly specific agent administered at varying times following the administration of either a ligand that exhibits competitive binding to the target, or a therapeutic that modulates the expression of the target, important information about the rate of target replenishment (i.e., receptor recycling) or the efficacy of therapy can be determined. Such analysis assumes the use of ''stealthy'' molecular contrast agents whose resistance to transport to the tissue region of interest do not limit the uptake process. Finally, the analogous molecular nuclear imaging technique of gamma scintigraphy requires several minutes for image acqui-

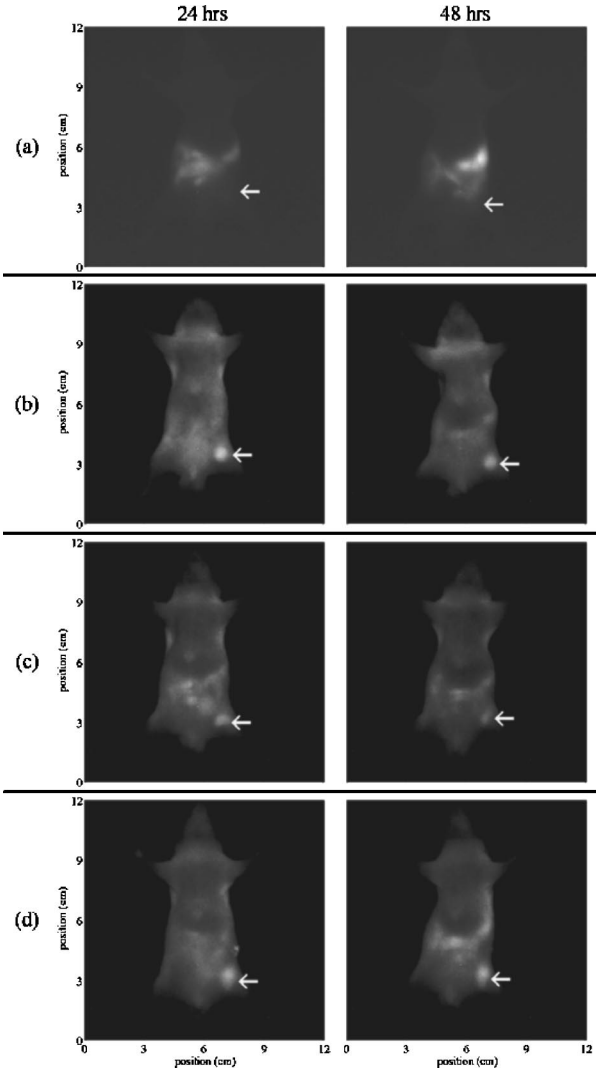

Fig. 6 Raw fluorescence images (no background subtraction) obtained 24 h (first column) and 48 h (second column) after the administration of (a) Cy5.5, (b) Cy5.5-c(KRGDf) conjugate alone, (c) Cy5.5-c(KRGDf) conjugate 1 h after the injection of RGD peptide, and (d) Cy5.5-c(KRGDf) conjugate 24 h after injection of the RGD peptide. The white arrows indicate the location of the xenografted Kaposi's sarcoma tumor.

sition in comparison to the subsecond image acquisition presented herein for dynamic optical imaging. Such temporal resolution for dynamic imaging suggests that optical imaging may not only join nuclear imaging as another ''gold standard'' of molecular imaging in medicine,[24] but may provide more quantitative information to assess the dynamics of disease marker expression.

In closing, until RTE-based tomographic algorithms are validated for small animal imaging, information on the biodistribution of optical contrast agents or fluorescently tagged molecules remain problematic and difficult. Until such a time that small animal tomography is validated, the simple approach presented herein for assessing uptake can provide a convenient and simple manner to confirm molecular specificity of the agent before biodistribution studies are undertaken. In yet another approach to the problem, we have dual labeled c(KRGDf) with both an optical and nuclear tracer in order to provide a validated means for assessing biodistribution.[24,25] While the dual labeled c(KRGDf) represents yet a different contrast agent targeting the same disease marker considered herein, it provides a new approach to perform both biostribution assessment in deep tissues from nuclear emission and pharmacokinetic information on surface tissue from optical emissions. Clearly the ability for rapid, dynamic optical imaging combined with proposed small animal optical tomography would enable the full complementary of information required for drug and contrast agent discovery without the need for dual labeling.

Acknowledgments

The authors gratefully acknowledge the support of the National Institutes of Health (NIH EB000174, EB003132, the Texas ATP Program (003657-0042-2001), and the John S. Dunn Research Foundation.

References

1. O. M. Fischer, S. Streit, S. Hart, and A. Ullrich, ''Beyond Herceptin and Gleevec,'' *Curr. Opin. Chem. Biol.* **7**, 490–495 (2003).
2. R. Abou-Jawde, T. Choueiri, C. Alemany, and T. Mekhail, ''An overview of targeted treatments in cancer,'' *Clin. Ther.* **25**, 2121–2137 (2003).
3. J. A. Kim, ''Targeted therapies for the treatment of cancer,'' *Am. J. Surg.* **186**, 264–268 (2003).
4. R. Roskoski, Jr., ''STI-571: an anticancer protein-tyrosine kinase inhibitor,'' *Biochem. Biophys. Res. Commun.* **309**, 709–717 (2003).
5. T. J. Heiken, M. Farolan, S. G. Ronan, A. Shilkaitis, L. Wild, and T. K. D. Gupta, ''β3 Integrin expression in melanoma predicts subsequent metastasis,'' *J. Surg. Res.* **63**, 169–173 (1996).
6. P. C. Brooks, R. A. F. Clark, and D. A. Cheresh, ''Requirement of vascular integrin $\alpha_v\beta_3$ for angiogenesis,'' *Science* **264**, 569–571 (1994).
7. P. C. Brooks, S. Stromblad, R. Klemke, D. Visscher, F. H. Sarkar, and D. A. Cheresh, ''Anti-integrin $\alpha_v\beta_3$ blocks human breast cancer growth and angiogenesis in human skin,'' *J. Clin. Invest.* **96**, 1815–1822 (1995).
8. C. L. Kumar, M. Malkowski, Z. Yin, E. Tanghetti, B. Yaremko, T. Nechuta, J. Varner, M. Liu, E. M. Smith, B. Neustadt, M. Prestam, and L. Armstrong, ''Inhibition of angiogenesis and tumor growth by SCH221153, a dual $\alpha_v\beta_3$ and $\alpha_v\beta_5$ integrin receptor antagonist,'' *Cancer Res.* **61**, 2232–2238 (2001).
9. J. C. Gutheil, T. N. Campbell, P. R. Pierce, J. D. Watkins, W. D. Huse, D. J. Bodkin, and D. A. Cheresh, ''Targeted antiangiogenic therapy for cancer using Vitaxin: a humanized monoclonal antibody to the integrin $\alpha_v\beta_3$,'' *Clin. Cancer Res.* **6**, 3056–3061 (2000).
10. F. A. L. M. Eskens, H. Dumez, R. Hoekstra, A. Perschl, C. Brindley, S. Böttcher, W. Wynendaele, J. Drevs, J. Verweij, and A. T. Oosterom, ''Phase I and pharmacokinetic study of continuous twice weekly intravenous administration of Cilengitide (EMD 121974), a novel inhibitor of the integrins $\alpha_v\beta_3$ and $\alpha_v\beta_5$ in patients with advanced solid tumours,'' *Eur. J. Cancer* **39**, 917–926 (2003).
11. D. A. Sipkins, D. A. Cheresh, M. R. Kazemi, L. M. Nevin, M. D. Bednarski, and K. C. P. Li, ''Detection of tumor angiogenesis *in vivo* by $\alpha_v\beta_3$-targeted magnetic resonance imaging,'' *Nat. Med.* **4**, 623–626 (1998).
12. R. Haubner, H.-J. Wester, U. Reuning, R. Senekowitsch-Schmidtke, B. Diefenbach, H. Kessler, G. Stocklin, and M. Schwaiger, ''Radiolabeled $\alpha_v\beta_3$ integrin antagonists: a new class of tracers for tumor targeting,'' *J. Nucl. Med.* **40**, 1061–1071 (1999).
13. R. Haubner, H.-J. Wester, W. A. Weber, C. Mang, S. I. Ziegler, S. L. Goodman, R. Senekowitsch-Schmidtke, H. Kessler, and M. Schwaiger, ''Noninvasive imaging of $\alpha_v\beta_3$ integrin expression using ^{18}F-labeled RGD-containing glycopeptide and positron emission tomography,'' *Cancer Res.* **61**, 1781–1785 (2001).

14. M. L. Janssen, W. J. Oyen, I. Dijkgraaf, L. F. Massuger, C. Frielink, S. Edwards, M. Rajopadhye, H. Boonstra, F. H. Corstens, and O. C. Boerman, ''Tumor targeting with radiolabeled $\alpha_v\beta_3$ integrin binding peptides in a nude mouse model,'' *Cancer Res.* **62**, 6146–6151 (2002).
15. W. Wang, S. Ke, Q. Wu, C. Charnsangavej, M. Gurfinkel, J. G. Gelovani, E. M. Sevick-Muraca, and C. Li, ''Near-infrared optical imaging of integrin $\alpha_v\beta_3$ in Human Tumor Xenografts,'' *Molecular Imaging* (in press).
16. S. Ke, X. Wen, M. Gurfinkel, C. Charnsangavej, Z. Fan, S. Wallace, E. Sevick-Muraca, and C. Li, ''Near-infrared optical imaging of epidermal growth factor receptors (EGFr) in a breast cancer xenograft,'' *Cancer Res.* **63**, 7870–7875 (2003).
17. D. Cuccia, F. Bevilacqua, A. Durkin, S. Merritt, B. Tromberg, G. Gulsen, H. Yu, J. Wang, and O. Nalcioglu, ''*In vivo* quantification of optical contrast agent dynamics in rat tumors by use of diffuse optical spectroscopy with magnetic resonance imaging coregistration,'' *Appl. Opt.* **42**, 2940–2950 (2003).
18. M. Gurfinkel, A. Thompson, W. Ralston, T. Troy, A. Moore, T. Moore, J. Gust, D. Tatman, J. Reynolds, B. Muggenburg, K. Nikula, R. Pandey, R. Mayer, D. Hawrysz, and E. Sevick-Muraca, ''Pharmacokinetics of ICG and HPPH-car for the detection of normal and tumor tissue using fluorescence, near-infrared reflectance imaging: a case study,'' *Photochem. Photobiol.* **72**, 94–102 (2000).
19. A. Godavarty, M. J. Eppstein, C. Zhang, S. Theru, A. B. Thompson, M. Gurfinkel, and E. M. Sevick-Muraca, ''Fluorescence-enhanced optical imaging in large tissue volumes using a gain modulated ICCD camera,'' *Phys. Med. Biol.* **48**, 1701–1720 (2003).
20. A. Godavarty, A. B. Thompson, R. Roy, M. Gurfinkel, M. J. Eppstein, C. Zhang, and E. M. Sevick-Muraca, ''Diagnostic Imaging of breast cancer using fluorescence-enhanced optical tomography,'' *J. Biomed. Opt.* **9**(3), 488–496 (2004).
21. A. Godavarty, A. B. Thompson, R. Roy, M. J. Eppstein, C. Zhang, and E. M. Sevick-Muraca, ''Detection of multiple targets in breast phantoms using fluorescence enhanced optical imaging,'' *Radiology* **235**, 148–154 (2005).
22. R. Roy, A. B. Thompson, A. Godavarty, and E. M. Sevick-Muraca, ''Tomographic fluorescence imaging in tissue phantoms: a novel reconstruction algorithm and imaging geometry,'' *IEEE Trans. Med. Imaging* **24**(2), 137–154 (2005).
23. R. Roy, A. Godavarty, and E. M. Sevick-Muraca, ''Fluorescence-enhanced optical tomography of a large tissue phantom using point illumination geometry,'' *J. Biomed. Opt.* (submitted).
24. J. P. Houston, S. Ke, W. Wang, C. Li, and E. M. Sevick-Muraca, ''Quality analysis of *in vivo* NIR fluorescence and conventional gamma images acquired using a dual-labeled tumor-targeting probe,'' *J. Biomed. Opt.* (submitted).
25. S. Ke, W. Wang, Q. Wu, C. Charnsangavej, J. P. Houston, D. Chow, E. M. Sevick-Muraca, and C. Li, ''Dual optical and nuclear imaging of integrin $\alpha_v\beta_3$ in human melanoma xenografts using a single imaging probe,'' *Eur. J. Nuc. Med. Mol. Imag.* (submitted).